The Astrophysical Journal, 828:100 (8pp), 2016 September 10 doi:10.3847/0004-637X/828/2/100

OUTFLOW DETECTION IN A 70 μm DARK HIGH-MASS CORE

Siyi Feng (冯思轶)[1,2], Henrik Beuther[2], Qizhou Zhang[3], Hauyu Baobab Liu (包包)[4], Zhiyu Zhang (张智昱)[4,5], Ke Wang (王科)[4], and Keping Qiu[6,7]
[1] Max-Planck-Institut für Extraterrestrische Physik, Gießenbachstraße 1, D-85748, Garching bei München, Germany; syfeng@mpe.mpg.de
[2] Max-Planck-Institut für Astronomie, Königstuhl 17, D-69117, Heidelberg, Germany
[3] Harvard-Smithsonian Center for Astrophysics, 60 Garden Street, Cambridge MA 02138, USA
[4] European Southern Observatory, Karl-Schwarzschild-Str. 2, D-85748, Garching bei München, Germany
[5] Institute for Astronomy, University of Edinburgh, Royal Observatory, Blackford Hill, Edinburgh EH9 3HJ, UK
[6] School of Astronomy and Space Science, Nanjing University, 22 Hankou Road, Nanjing 210093, China
[7] Key Laboratory of Modern Astronomy and Astrophysics (Nanjing University), Ministry of Education, Nanjing 210093, China
Received 2016 January 18; revised 2016 May 3; accepted 2016 May 5; published 2016 September 8

ABSTRACT

We present observations toward a high-mass (>40 $M_\odot$), low-luminosity (<10 $L_\odot$) 70 μm dark molecular core G28.34 S-A at 3.4 mm, using the IRAM 30 m telescope and the NOEMA interferometer. We report the detection of SiO $J = 2 \rightarrow 1$ line emission, which is spatially resolved in this source at a linear resolution of ~0.1 pc, while the 3.4 mm continuum image does not resolve any internal sub-structures. The SiO emission exhibits two W–E oriented lobes centering on the continuum peak. Corresponding to the redshifted and blueshifted gas with velocities up to 40 km s^{-1} relative to the quiescent cloud, these lobes clearly indicate the presence of a strong bipolar outflow from this 70 μm dark core, a source previously considered as one of the best candidates of "starless" core. Our SiO detection is consistent with ALMA archival data of SiO $J = 5 \rightarrow 4$, whose high-velocity blueshifted gas reveals a more compact lobe spatially closer to the dust center. This outflow indicates that the central source may be in an early evolutionary stage of forming a high-mass protostar. We also find that the low-velocity components (in the range of $V_{lsr}^{+3}_{-5}$ km s^{-1}) have an extended, NW–SE oriented distribution. Discussing the possible accretion scenarios of the outflow-powering young stellar object, we argue that molecular line emission and the molecular outflows may provide a better indication of the accretion history of the forming young stellar object, than snapshot observations of the present bolometric luminosity. This is particularly significant for cases of episodic accretion, which may occur during the collapse of the parent molecular core.

Key words: ISM: lines and bands – stars: formation – stars: massive – submillimeter: ISM

1. INTRODUCTION

Whether high-mass stars form via a quick global collapse of a dense molecular gas core, followed by the formation of a stellar object (Tan & McKee 2002; McKee & Tan 2003; Krumholz & Bonnell 2007; Gong & Ostriker 2011; Kuiper & Klessen 2013), or whether they form via competitive accretion of a cluster of low-mass (proto)stars (Bonnell et al. 2001, 2004, 2007), remains a fundamental question in the field of high-mass cluster formation (Tan et al. 2014). Identifying and then resolving the initial conditions of high-mass star formation is the first step toward addressing this question (e,g., Zhang et al. 2009). Candidates of initial high-mass star-forming regions are expected to be embedded in the dense ($n \geqslant 10^3$–10^5 cm^{-3}; Teyssier et al. 2002; Rathborne et al. 2006; Butler & Tan 2009; Ragan et al. 2009; Vasyunina et al. 2009; Wang et al. 2011), cold ($T < 20$ K; Carey et al. 1998; Sridharan et al. 2005; Pillai et al. 2006; Wang et al. 2008, 2012; Wienen et al. 2012; Chira et al. 2013), and low-luminosity molecular clouds, which have high dust extinction and short free-fall collapse timescales (on the order of 5×10^4 year, e.g., Russeil et al. 2010; Tackenberg et al. 2012). The so-called IR-dark molecular clouds (IRDCs) unveiled by the previous *Midcourse Space Experiment* (e.g., Egan et al. 1998; Simon et al. 2006) and *Spitzer* near-mid IR survey (e.g., GLIMPSE, Robitaille et al. 2008; Cyganowski et al. 2008; MIPSGAL, Carey et al. 2009), have provided excellent road maps to look for these objects.

The 70 μm dark molecular clump G28.34 S (Ragan et al. 2012, 2013) was discovered around the southern edge of the filamentary IRDC G28.34+0.06 (~4.7 kpc, Carey et al. 1998, 2000, Figures 1(a) and (b)). Previous studies revealed that this source has a high molecular gas density (>10^5 cm^{-3}, Butler & Tan 2009), a low luminosity with a starless-core-like spectral energy distribution (SED; 10 $L_\odot$, Ragan et al. 2013), a low temperature (13–16 K from the SABOCA 350 survey and SPIRE 500), and high deuteration (Chen et al. 2010; Fontani et al. 2011), indicating its early evolutionary stage. Our previous observations (Feng et al. 2016) toward this region further indicated a high ionization ratio (>10^{-7}), a large number of nitrogen bearing species, and significant CO depletion (~15, Figure 1(c)). The latter is strongly supported by an anti-correlated distribution between CO and N_2H^+/NH_2D/$H^{13}CO^+$ on scales of 0.8 pc. In fact, this region has been considered as one of the best candidates for hosting two high-mass starless cores (e.g., Chen et al. 2010; Tan et al. 2013; Kong et al. 2016). However, surprisingly we found >5σ emission of SiO $J = 2 \rightarrow 1$ with >0.2 pc extent in a 30 m line survey (Feng et al. 2016). This line emission, coincident with a varying H_2O maser (Wang et al. 2006, 2012), suggested that star formation may have already begun.

Outflows are usually considered important to distinguish between prestellar and protostellar objects. While low-velocity SiO may be released to the gas-phase by large-scale mechanisms such as cloud–cloud collisions (Jiménez-Serra et al. 2009, 2010), the high-velocity SiO (with broad line wings >20 km s^{-1}) regularly observed in high-mass protostars is commonly used to reveal outflows (e.g., Schilke et al. 1997;

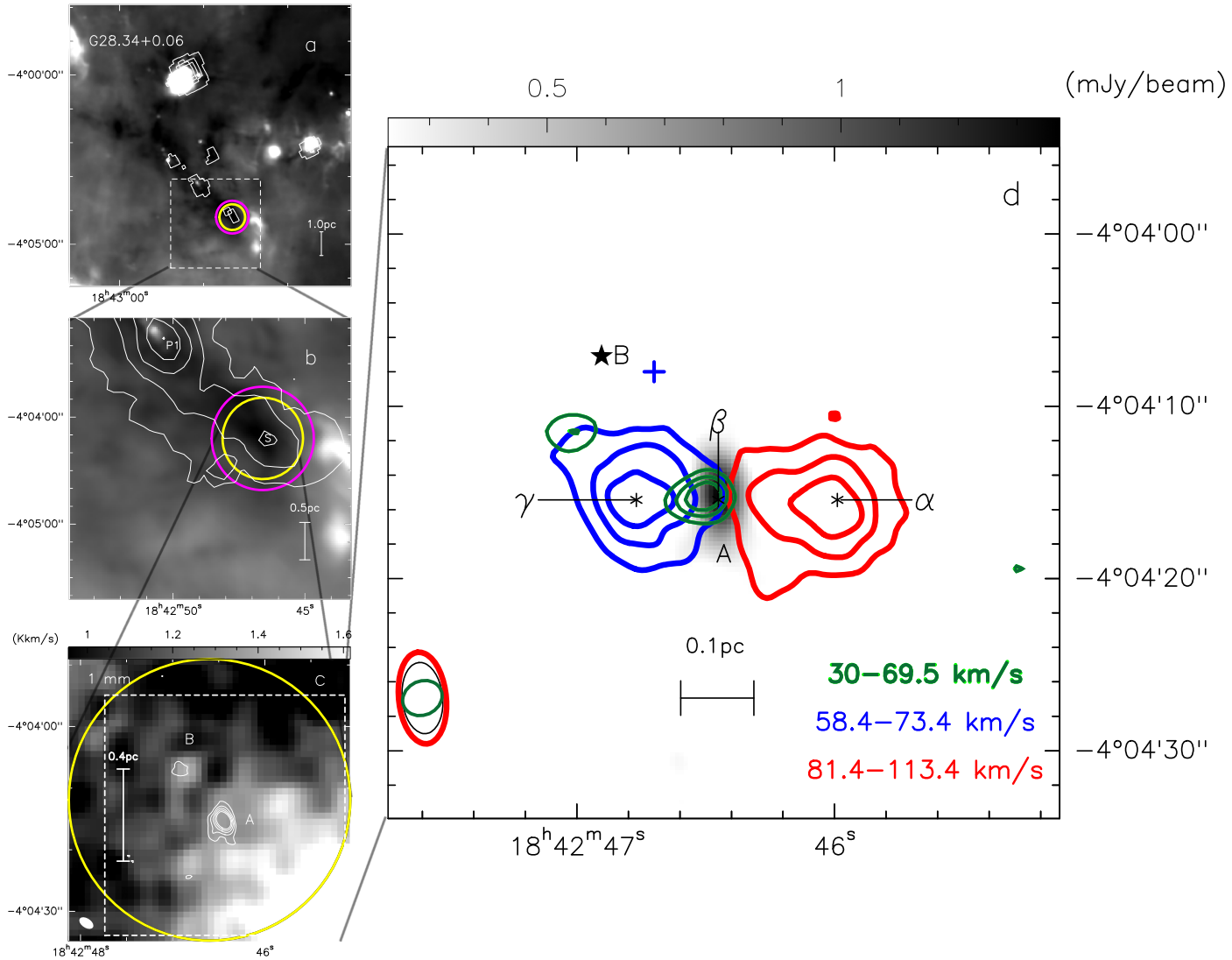

Figure 1. Compilation of the observations on G28.34 S. (a) and (b) Grayscale map of the dust emission observed by *Herschel* at 70 μm (Ragan et al. 2012). The white contours show continuum emission observed by ATLASGAL at 870 μm (Schuller et al. 2009). White contours in (a) start from 15σ rms and continue in 15σ rms steps (σ = 50 mJy/beam) and in (b) they start from 5σ rms and continue in 5σ rms steps. We mark two continuum peaks: P1 (Wang et al. 2011, 2012) and S (our targeted source). (c) White contours show the continuum observed by the SMA COMP configuration at 1.1 mm, overlaying the moment 0 grayscale map of highly depleted (~15) $C^{18}O$ $J = 2 \rightarrow 1$ (integrated through its FWZI) from IRAM 30 m observations. Contours start from 5σ rms and continue in 5σ rms steps (σ = 1 mJy/beam). (d) Grayscale map of the continuum observed by NOEMA at 3.4 mm. Red and blue contours show the red/blueshifted gas of SiO $J = 2 \rightarrow 1$ (V_{lsr} = 78.4 km s^{-1}) obtained from the combination of NOEMA and 30 m observations. The integration range covers the entire red/blueshifted line wing. The green contours show the blueshifted gas of SiO $J = 5 \rightarrow 4$ from ALMA Cycle 0 public data (the velocity range is only covered up to 69.5 km s^{-1} by observations). α, β, and γ mark the emission peak of the redshifted lobe, the continuum peak, and the emission peak of the blueshifted lobe, respectively. All the colored contours in figure (d) start from 4σ rms and continue in 4σ rms steps (σ = 88 mJy/beam, red; 49 mJy/beam, blue; 35 mJy/beam, green). The blue cross denotes the H_2O maser at 59.5 km s^{-1} (Wang et al. 2006). In figures (b) and (c), the SMA/NOEMA/NOEMA+30 m synthesized beam is in the bottom left. The yellow circle show the primary beam of SMA at 1.1 mm, the magenta circle shows the primary beam of NOEMA at 3.4 mm.

Beuther et al. 2004; Qiu et al. 2007; Liu et al. 2012; Duarte-Cabral et al. 2014; López-Sepulcre et al. 2016). Therefore, the line profile of SiO on the core scale (0.1 pc) is crucial to judge whether protostellar object(s) are already in the 70 μm dark G28.34 S.

Here we present direct evidence for a spatially resolved molecular outflow in the high-mass molecular gas core G28.34 S-A (hereafter S-A[8], Figure 1(c)), using the combined Northern Extended Millimeter Array (NOEMA) and IRAM 30 m telescope observations of the SiO $J = 2 \rightarrow 1$ line.

2. OBSERVATIONS AND ARCHIVAL DATA

2.1. NOEMA

To explore the spatial origin of this strongly emitting SiO $J = 2 \rightarrow 1$ line, we observed G28.34 S using NOEMA at 87.7 GHz (3.4 mm) in its B (with 6–7 working antennae on different days), C (5 antennae), and D (5–6 antennae) configurations from 2015 March 21 to May 23. With projected baselines of 24–404 m, the observations are sensitive to structures up to 18″, and the primary beam is 58″ at 3.4 mm.

[8] The entire G28.34 S region corresponds to the "leaf" No. 5 from dendrogram of SABOCA 350 μm in Ragan et al. (2013). S-A and S-B in this paper correspond to C1-S and C1-N in Tan et al. (2013); S-A corresponds to MM9 in Rathborne et al. (2006) and Chen et al. (2010).

For all observations a common phase center was used, at $18^h42^m46^s.597$, $-04°04'11''.940$ (J2000). The precipitable water vapor varied between 2 and 6 mm during the observations. Standard interferometric calibrations were performed during the observations, using quasars 1741–038 and 1827+062 as gain calibrators, 3C 273 or 0923+392 as the bandpass calibrator, and MWC 349, 1749+096, or 3C 273 as the flux calibrator. The uncertainty of absolute flux scale is estimated to be correct to within ~5%.

SiO $J = 2 \rightarrow 1$ was covered by a narrow-band correlator unit with a channel width of 0.078 MHz (0.275 km s^{-1}). Continuum emission was observed by the wide-band receiver (WIDEX), covering 85.9–89.5 GHz with a channel width of 1.95 MHz. Data calibration is performed using the GILDAS[9] package. The 3.4 mm continuum image is made by averaging the line-free channels of the WIDEX band. We used the natural weighting to achieve a better signal-to-noise ratio. The final 3.4 mm continuum image has a synthesized beam of $4''.15 \times 2''.35$ (PA $= -171°$) and the 1σ rms value is 0.08 mJy beam^{-1}.

2.2. IRAM 30 m Telescope

To compensate the missing flux, we use data from an imaging line survey on G28.34 S with the IRAM 30 m telescope at 3 mm (see details in Feng et al. 2016). Observations were performed in the on-the-fly mode on 2014 May 28, mapping a $1'.5 \times 1'.5$ area centered at $18^h42^m46^s.597$, $-04°04'11''.940$ (J2000). A broad bandpass (8 GHz bandwidth) covers the range of 85.8–93.6 GHz with a frequency resolution of 0.195 MHz (velocity resolution of 0.641 km s^{-1} at 3 mm). The FWHM beam of the 30 m telescope is ~30″ at 3 mm. The 1σ rms T_{mb} in the line-free channels is 6–8 mK at 3 mm. At such sensitivity, the extent of the $>5\sigma$ emission of SiO $J = 2 \rightarrow 1$ is >0.2 pc.

We combined the large-scale SiO $J = 2 \rightarrow 1$ obtained from the IRAM 30 m telescope with the high resolution data from NOEMA using GILDAS. The combined SiO line cube has a synthesized beam of $5''.35 \times 2''.76$ (PA $= -174°$). The spectral resolution is smoothed to 1 km s^{-1} and the 1σ rms value is 6.1 mJy beam^{-1}.

2.3. Submillimeter Array (SMA)

Observations with the SMA[10] (Ho et al. 2004) were carried out in the extended (EXT) and compact (COMP) configurations at 260/270 GHz (1.1 mm) on 2013 June 11 and July 19, respectively. The primary beam is 48″, and the baseline range is 16–226 m, sensitive to structures up to 10″. The correlator was tuned to cover 258.1–262.0 GHz in the lower side band and 270.0–273.9 GHz in the upper side band, with a uniform channel width of 0.812 MHz (0.936 km s^{-1}). More details of the observations and data calibration are given in Feng et al. (2016).

No line is detected in the image domain, although a 2.5σ signal of SiO $J = 6 \rightarrow 5$ is seen in the (u,v) spectrum. We made continuum images using data from the combined COMP+EXT data ($2''.55 \times 1''.51$, PA $= 33°$, Figure 1(c)). The 1σ rms value is 0.97 mJy beam^{-1}.

2.4. ALMA Archival Data

We further obtained archival data observed with ALMA. The project number is 2011.0.00236.S, and was carried out with the compact configuration in ALMA Cycle 0. The details of the observations can be found in Tan et al. (2013). We downloaded the calibrated data from the ALMA archive and cleaned it with natural weighting in CASA (McMullin et al. 2007). The derived angular resolution is $2''.35 \times 1''.98$ (PA $= -66°$), and the maximum detectable scale is ~9″. The rms noise level is ~7.4 mJy per 0.08 km s^{-1} channel after continuum subtraction. Unfortunately the bandpass only covers part of the blueshifted velocity range (<69.5 km s^{-1}) of the SiO $J = 5 \rightarrow 4$ emission.

3. RESULTS

3.1. Spatial Distribution of SiO Emission

Figure 1(d) shows the 0.06 pc resolution, 3.4 mm continuum image of S-A (grayscale), overlaid with the velocity-integrated SiO $J = 2 \rightarrow 1$ flux intensities (contours). The 3.4 mm continuum image resolves a single dust component, which has a 2D Gaussian deconvolved size scale of ~0.08 pc ($5''.04 \times 2''.62$, PA $= 92°$). In addition, we detected high-velocity blueshifted and redshifted gas lobes in SiO $J = 2 \rightarrow 1$, which are associated with the 3.4 mm continuum in the W–E orientation. The 2D Gaussian deconvolved size of the blueshifted and redshifted gas lobes are $6''.42 \times 5''.48$ (PA $= 55°$) and $7''.76 \times 5''.82$ (PA $= 98°$), respectively.

The blueshifted gas lobe seen in SiO $J = 5 \rightarrow 4$ appears more compact ($2''.9 \times 2''.2$, PA $= 108°$ after 2D Gaussian deconvolution). It is closer to the 3.4 mm continuum center than SiO $J = 2 \rightarrow 1$ by 2″. This is likely due to a higher excitation condition requirement of the SiO $J = 5 \rightarrow 4$ line, which better traces a localized warmer part of the blueshifted gas. The ALMA data also provide a better sensitivity than the NOEMA-30 m observations[11], so it can detect the highest velocity line wing of the outflow which is not seen in the NOEMA-30 m data.

3.2. Position–Velocity (PV) Diagram

To study the velocity distributions of two SiO lines along the W–E extension, we convolve the $J = 5 \rightarrow 4$ data obtained with ALMA to the same angular resolution as the $J = 2 \rightarrow 1$ data obtained with NOEMA. To increase the signal-to-noise ratio, we take a 5″-width slice along the W–E orientation and extract a PV diagram from both lines (Figure 2 left panel), using the "pvextractor" code.[12] The PV diagram of both SiO transitions reveals that the higher velocity components are located closer to the continuum peak while the lower velocity components are further away from the continuum. This is probably due to two factors, the first of which is the excitation conditions. The highest velocity gas near the continuum peak might have a higher excitation with a higher temperature and density. The high-J SiO lines could be enhanced by the high-velocity shocks, while the low-J lines are from the entrained cocoon which has lower velocities (see the similar case in HH 211;

[9] http://www.iram.fr/IRAMFR/GILDAS

[10] The Submillimeter Array is a joint project between the Smithsonian Astrophysical Observatory and the Academia Sinica Institute of Astronomy and Astrophysics, and is funded by the Smithsonian Institution and the Academia Sinica.

[11] The ALMA $J = 5 \rightarrow 4$ observation is ~5.5 times more sensitive than the NOEMA-30 m $J = 2 \rightarrow 1$ observations in detecting the outflow mass, when smoothing both data into the same spatial and velocity resolution and assuming the same gas temperature of 15 K.

[12] http://pvextractor.readthedocs.org

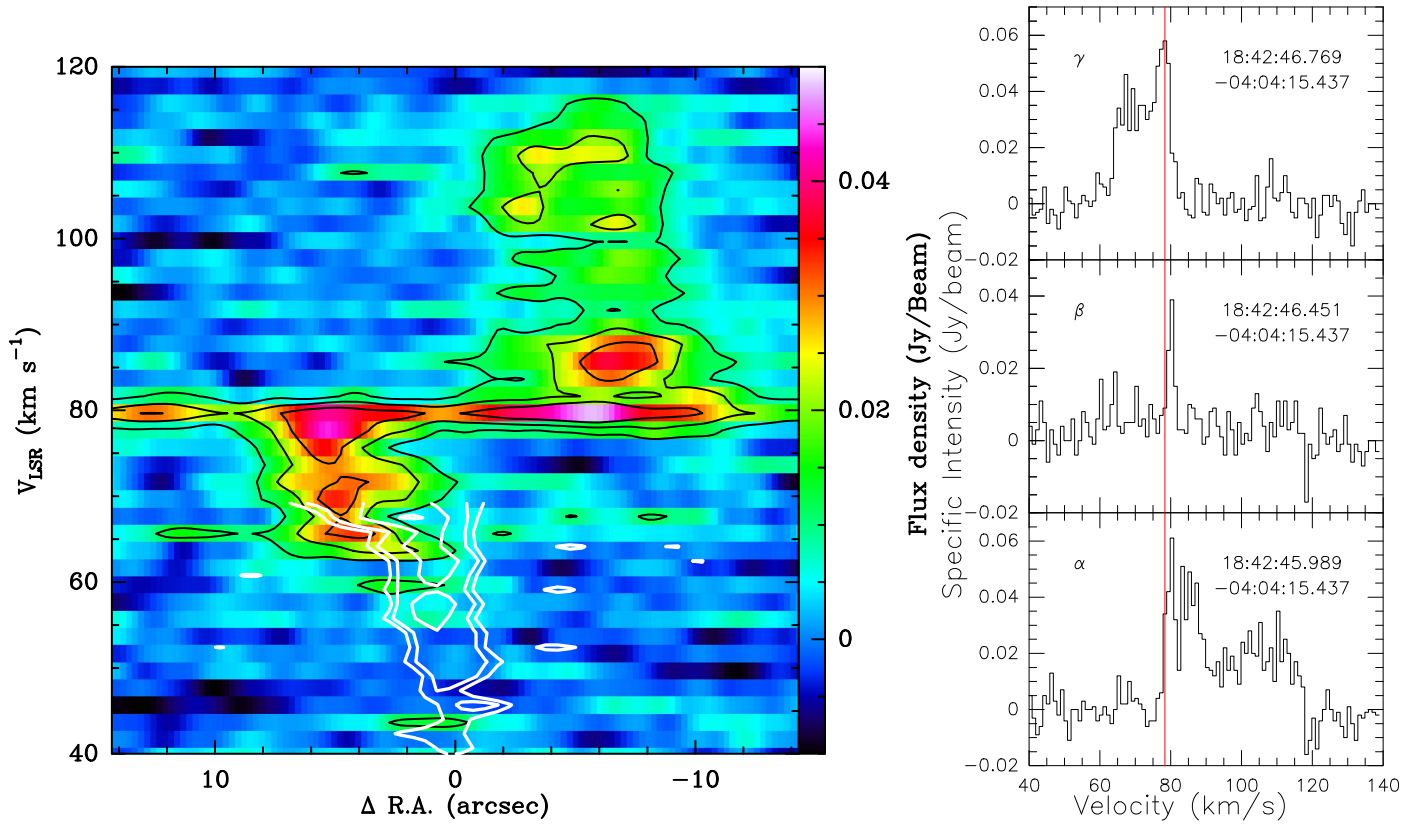

Figure 2. Left panel: PV diagram along the W–E orientation with a width of 5″. The colormap and the black contours are extracted from the SiO $J = 2 \rightarrow 1$ line, with contour levels of 0.01, 0.02, and the 0.03 Jy beam^{-1}. The white contours are from the SiO $J = 5 \rightarrow 4$ line (velocity coverage up to 69.5 km s^{-1} by ALMA observations), with contour levels of 0.006, 0.01, and 0.02 Jy beam^{-1}. Note that the ALMA data have been convolved to the same angular resolution of the NOEMA data for comparison. Right panel: line profiles extracted from the positions marked in Figure 1(d).

Hirano et al. 2006; Palau et al. 2006; Lee et al. 2007). The second reason is a mechanical effect. It is also possible that the central protostar ejects outflows episodically, and later ejecta have higher velocities; or, the outflow is still in an early stage and the shock front decelerates because of its interaction with the ambient gas. These may bring in spatially differentiated velocity components from the same transition ($J = 2 \rightarrow 1$).

3.3. SiO Line Profiles: Toward/Away from the Dust Core

Line profiles of SiO $J = 2 \rightarrow 1$ vary spatially (Figure 2 right panel). Narrow line emission (FWZI, the overall zero-intensity velocity dispersion of $\sim$4 km s^{-1}) with $\sim$+2 km s^{-1} shifted from the V_{lsr} of the cloud is detected toward the continuum center. In contrast, the line profiles of SiO $J = 2 \rightarrow 1$ toward the emission peak of the blue/redshifted lobes are broader (FWZI >30 km s^{-1}). Each profile has double intensity peaks: a more intensive peak with a narrow FWHM linewidth around the V_{lsr} and a higher velocity peak with broader line wings. Such profiles perfectly match the prediction of the evolutionary SiO line profiles introduced by C-shock models at the core scale (Jiménez-Serra et al. 2009). The low-temperature neutral fluid at the young, magnetic precursor stage produces the narrow line, and a small ion-neutral drift velocity leads to the sputtering of the grain mantles. Shock propagation and heating broaden the line profiles in the lobes. The more intensive peak at lower velocity is related to the silicon ejected from the grain, while the less intensive peak at higher velocity corresponds to the large accumulation of SiO in the postshock.

The above observation results indicate that SiO emissions trace the shocked gas when the W–E oriented outflow impacts on the ambient gas. In addition to the outflow, other possible enriching mechanisms of SiO include vaporization and shattering by grain–grain collisions (e.g., Caselli et al. 1997; Guillet et al. 2009, 2011; Anderl et al. 2013) and cloud–cloud collisions (e.g., Jiménez-Serra et al. 2009, 2010; Nguyen-Lu'o'ng et al. 2013). However, previous observations and the current observations do not provide evidence for these mechanisms. For example, neither obvious velocity gradients of SiO nor temperature gradients in NH_3 (Wang et al. 2008) are detected on larger scales (>1 pc).

4. DISCUSSION

In the following discussion, we provide quantitative derivations of the physical properties of the unresolved high-mass molecular gas core (Section 4.1) of the the W–E oriented SiO outflow (Section 4.2) and of the low-velocity (<5 km s^{-1}) SiO emission (Section 4.3). We also discuss the physical implication of the derived quantities in Section 4.4.

4.1. Core Mass

Previous studies have indicated that S-A is a cold and dense gas core. Therefore, it is safe to assume that dust and gas are thermalized, such that dust temperature is equal to gas kinetic temperature (e.g., Juvela & Ysard 2011). Using the combined VLA+Effelsberg NH_3 lines (resolution of 5″, Wang

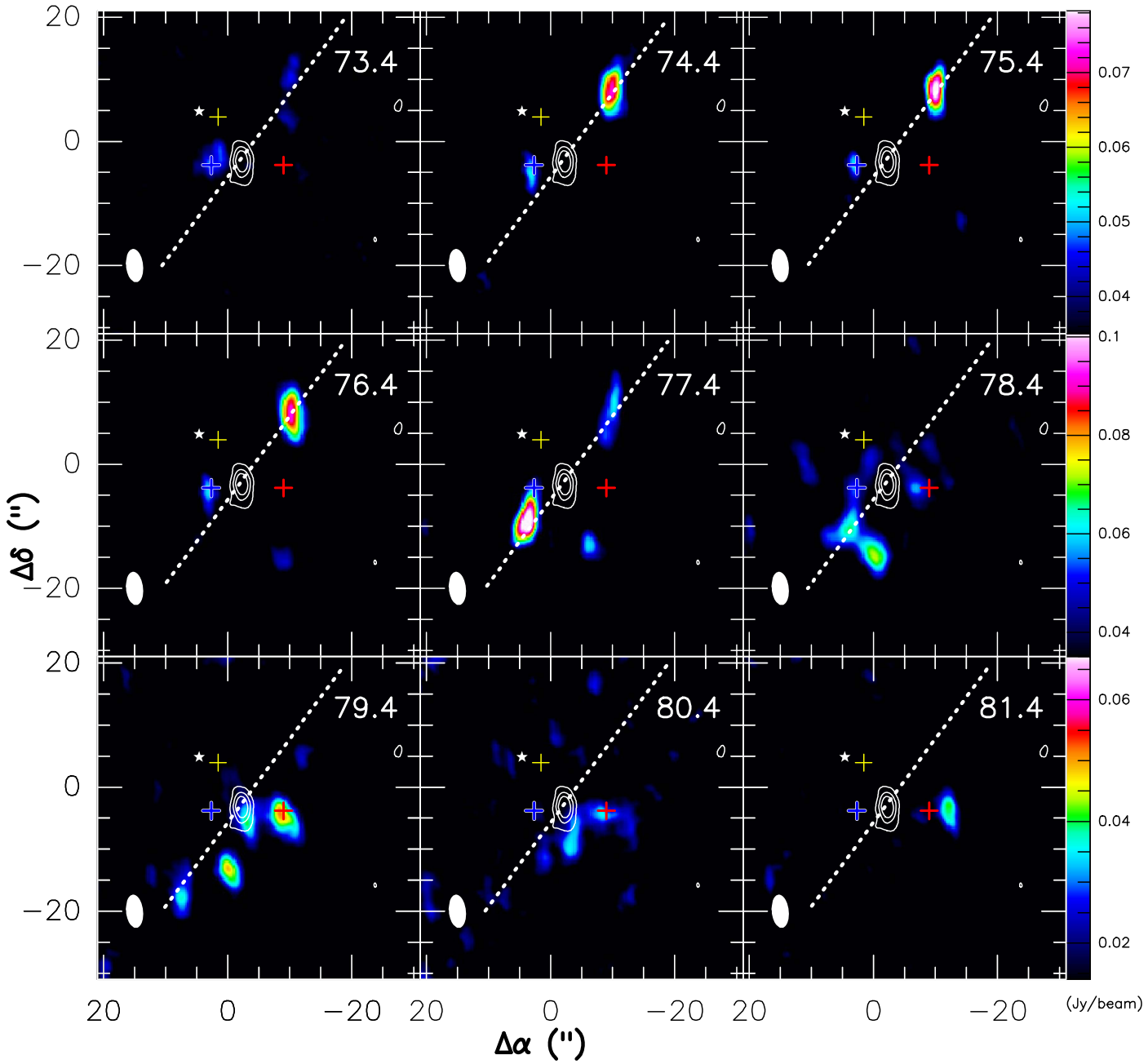

Figure 3. Channel maps of SiO $J = 2 \rightarrow 1$ (colormap) in the velocity range of Vlsr^{+3}_{-5} km s^{-1}. The white contours show the 3.4 mm continuum emission. The blue (red) cross shows the blueshifted (redshifted) gas lobe. The yellow cross denotes the H_2O maser. The star marks the 1.2 mm continuum source S-B. The white dashed line indicates the elongation of the NW–SE structure.

et al. 2008) and the procedure outlined in Wang et al. (2014), we fit a gas kinetic temperature of $T_{\rm kin} \approx 15$ K for S-A.

We assume that the 1.1 and 3.4 mm continuum emission is dominated by thermal dust emission. Adopting a gas-to-dust mass ratio of 150 (Draine 2011), a dust opacity of $\kappa_{1.1\,\rm mm} = 1.0\,\rm cm^2\,g^{-1}$ and $\kappa_{3.4\,\rm mm} = 0.17\,\rm cm^2\,g^{-1}$ ($\kappa \propto \nu^{1.8}$, Ossenkopf & Henning 1994), we estimate a core mass of $\sim 40\,M_\odot$ ($\sim 53\,M_\odot$), a H_2 column density of $\sim 5 \times 10^{23}\,\rm cm^{-2}$ ($\sim 6 \times 10^{23}\,\rm cm^{-2}$), and a number density $n \sim 3 \times 10^6\,\rm cm^{-3}$ ($\sim 5 \times 10^6\,\rm cm^{-3}$) in the unresolved core S-A, from the 3.4 mm (1.1 mm) continuum, obtained with NOEMA (SMA). Comparing to the 870 μm single-dish continuum emission and assuming a spectral index in the range of 3.5–4, more than 60% of the missing flux leads to the above core mass being a lower limit. Our constraints on the gas number density imply a free-fall collapsing timescale shorter than $t_{\rm ff} = 3.66 \times 10^7/\sqrt{n}$ yr $\sim 10^5$ yr. Dividing core mass by the free-fall collapsing timescale, the inferred averaged accretion rate is $10^{-3}\,M_\odot\rm yr^{-1}$ or higher.

4.2. Physical Properties of the W–E Oriented Outflow

The entire G28.34 S region has a low bolometric luminosity $L_{\rm bol} \sim 10\,L_\odot$ (S. Ragan 2016, private communication). Assuming that this luminosity is mainly due to accretion of a single young stellar object, the present mass of the central stellar object in S-A is likely in the range of

$0.1\,M_\odot \lesssim M_* < 3\,M_\odot$ (Dunham & Vorobyov 2012; Krumholz et al. 2014). The possible radius of the host (proto)star R_* ranges from 1.5 $R_\odot$ (Stahler et al. 1980) to several tens of $R_\odot$ (e.g., Hosokawa et al. 2010, 2011). The present accretion rate may range as follows, $\dot{M}_{\rm acc} < L_{\rm bol}R_*/(GM_*) = 10^{-7}$–$10^{-5}\,M_\odot{\rm yr}^{-1}$.

The exact physical properties of the SiO outflows are as yet uncertain, due to the unknown SiO abundance with respect to H_2 ($\chi_{\rm SiO}$). However, $\chi_{\rm SiO}$ may be related to the evolutionary scenario of the host powering source, which can be estimated by the following discussion. Our estimations are based on two assumptions: (1) the shocked gas in the outflow is warmer than or at least has the same temperature as the core center (15 K); (2) SiO $J = 2 \rightarrow 1$ is optically thin.

Using 2D Gaussian fits to the gas lobes in Figure 1(d), we measure the SiO $J = 2 \rightarrow 1$ total flux of the redshifted lobe as 4.02 Jy and of the blueshifted lobe as 2.06 Jy. The H_2 gas mass of the double-side lobes $M_{\rm lobes} = M_{\rm red} + M_{\rm blue} = 2.1 \times 10^{-11}/\chi_{\rm SiO}\,M_\odot$.

Using the highest outflow velocity observed from SiO $J = 2 \rightarrow 1$ ($V_{\rm max}$, 58.4 km s^{-1} and 113.4 km s^{-1}) in each lobe and $V_{\rm lsr}$ (78.4 km s^{-1}), the momentum of the outflow is $P = M_{\rm red}|V_{\rm max,red} - V_{\rm lsr}| + M_{\rm blue}|V_{\rm max,blue} - V_{\rm lsr}| = 6.1 \times 10^{-10}/\chi_{\rm SiO}\,M_\odot$ km s^{-1}. The high-velocity components are closer to the dust center, so we assume that different velocity components form different layers of gas. Comparing the timescale t_i that each velocity component V_i has been through to form its layer, with projection length L_i from the continuum center ($t_i = L_i/|V_i - V_{\rm lsr}|$), we derive the maximum as the outflow dynamic timescale $t_{\rm dyn} \sim 10^4$ years, which is shorter than the free-fall collapsing timescale of the parent dense core (Section 4.1) by a factor of 10. This is consistent with the fact that the observed source may be so young that it is at the beginning of star formation.

Assume that the outflow is momentum driven by the underlying wind, which has a speed $V_{\rm w}$ on the same order as the Keplerian velocity at the stellar surface, $V_{\rm k} = \sqrt{GM_*/R_*}$ (Krumholz et al. 2005), i.e., in the range of 20–600 km s^{-1}. Taking $V_{\rm w} = 300$ km s^{-1}, the mass-loss rate to the wind is $\dot{M}_{\rm w} = P/(V_{\rm w}t_{\rm dyn}) = 4 \times 10^{-14}/\chi_{\rm SiO}\,M_\odot{\rm yr}^{-1}$. We adopt a double-side mass loading ratio ($\dot{M}_{\rm w}/\dot{M}_{\rm acc}$) in the range of 0.1–0.3 (Tan et al. 2014). Therefore, possible scenarios based on the assumption of a constant mass loading are:

(1) A dominant outflow-powering young stellar object, which has a relatively high mass (1–2 $M_\odot$), has already formed in this dense core. Assuming the typical radius of such object is several $R_\odot$, the observed low bolometric luminosity ($<10\,L_\odot$) requires the mass accretion rate to be not very high ($\dot{M}_{\rm acc} < 10^{-7}$–$10^{-6}\,M_\odot{\rm yr}^{-1}$). This will imply a low outflow mass and a high SiO abundance ($\chi_{\rm SiO} > 4 \times 10^{-7}$);

(2) If the powering young stellar object has a relatively low mass (0.1 $M_\odot$) and large radius (typically tens of $R_\odot$), and if the accretion dominates the low bolometric luminosity ($<10\,L_\odot$), the mass accretion rate should be high ($\dot{M}_{\rm acc} < 10^{-5}$–$10^{-4}\,M_\odot{\rm yr}^{-1}$). This will imply a high outflow mass and a low SiO abundance ($\chi_{\rm SiO} > 4 \times 10^{-10}$).

The second scenario may be less likely. Assuming that the gas–dust temperature in the continuum peak of S-A (position β in Figure 1(d) and Figure 2 right panel) is 15 K, the SiO abundance in this dense core peak is $\chi_{{\rm SiO},\beta} \sim 5 \times 10^{-12}$. The predominant SiO emission observed in the outflow regions over that observed from the dense core indicates a much higher SiO abundance in the outflows. The lower limit of the SiO abundance in the outflows given by the temperature lower limit assumption[13] (15 K), velocity-integrated SiO flux intensity, and the 3σ continuum intensity (e.g., at positions α and γ), is $\chi_{{\rm SiO},\alpha\sim\gamma} > 10^{-9}$, which is higher than the estimates given by the second scenario.

Considering the averaged accretion rate ($10^{-3}\,M_\odot{\rm yr}^{-1}$, see Section 4.1) and the maximum outflow dynamic timescale ($\sim 10^4$ yr), the assumed 1–2 $M_\odot$ young stellar object in the first scenario may be reasonable. However, the derived SiO abundance from the first scenario is slightly higher than that in other observed shocked regions (10^{-10}–10^{-7}; e.g., Mikami et al. 1992; Zhang et al. 1995; Hirano et al. 2001; Gusdorf et al. 2008; Leurini et al. 2014). It is also puzzling that the derived mass accretion rate is low. The issues of too high a SiO abundance and too low an accretion rate can be alleviated if we consider the following scenario:

(3) A dominant outflow-powering young stellar object with a relatively high mass (1–2 $M_\odot$) has already formed and is accreting episodically.[14] In such case, the luminosity and the mass accretion rate should be high in the region during the dominant outflow eruptions, while it is currently in a relatively quiescent status with luminosity and mass accretion rate being temporarily low (e.g., Liu et al. 2016). The potentially much higher averaged accretion rate in the past (up to $10^{-3}\,M_\odot{\rm yr}^{-1}$) can bring in a more reasonable SiO abundance. Better estimates of SiO abundance from future observations on multiple transitions of more molecular species, may help discern scenarios (1) and (3).

Although we cannot exclude that S-A just forms a few low-mass stars, the large gas reservoir is indicative of a high-mass star-forming core.

Finally, based on the aforementioned assumptions, if we take $\chi_{\rm SiO} \sim 10^{-7}$, the mass entrainment rate of the outflow is $M_{\rm lobes}/t_{\rm dyn} \sim 10^{-8}\,M_\odot{\rm yr}^{-1}$, the kinetic energy is $E_{\rm lobes} = 1/2\,(M_{\rm red}|V_{\rm max,red} - V_{\rm lsr}|^2 + M_{\rm blue}|V_{\rm max,blue} - V_{\rm lsr}|^2) \sim 2 \times 10^{42}$ erg, and the mechanical luminosity is $E_{\rm lobe}/t_{\rm dyn} \sim 10^{-3}\,L_\odot$. If we take $\chi_{\rm SiO} \sim 10^{-9}$, the above parameters should be two magnitudes higher. However, these values indicate that the W–E outflow from S-A is less intense than the typical outflows from the more evolved high-mass star-forming regions (Beuther et al. 2002; Arce et al. 2007; Zhang et al. 2015).

4.3. A Second Outflow?

In addition to the W–E oriented high-velocity outflow, we note that the spatial distribution of the low-velocity $J = 2 \rightarrow 1$ line emission shows a NW–SE elongation, which is almost perpendicular to the major axis of the large-scale filament. Channel maps in the velocity range of $V{\rm lsr}^{+3}_{-5}$ km s^{-1} reveal a second pair of bright blueshifted and redshifted gas lobes,

[13] Temperature in the outflow may be enhanced (>15 K) because of the shocks (e.g., López-Sepulcre et al. 2016).

[14] Episodic accretion may occur when the gas core is collapsing onto the forming, approximately Keplerian-rotating disk. If the mass accretion onto the disk is much faster than the accretion rate of the host (proto)star, which is very likely to be the case during the collapsing phase, then the accumulated mass can make the disk become Toomre unstable (Toomre 1964), which triggers gravitational instability and episodic accretion (e.g., Vorobyov et al. 2013; Vorobyov & Basu 2015; Liu et al. 2016). The episodic scenario therefore may imply a forming high-mass star accreting via a Keplerian-rotating disk (see also Johnston et al. 2015). A immediate consequence of the potential episodic accretion is that the bolometric luminosity may not always be a good indicator for the evolutionary stage.

which are centered on the unresolved 3.4 mm continuum peak and are aligned at a position angle of PA $\sim -53°$ (Figure 3). The channel maps further indicate that the SE lobe is coincident with the blueshifted lobe of the W–E outflow at $\sim$77.4 km s^{-1}. Its origin is uncertain, but possible mechanisms for this elongation could be (1) a second outflow from the unresolved protostar(s) in S-A and (2) large-scale shock remnants (Jiménez-Serra et al. 2004). Although there is no significant evidence to rule out the second possibility, the gas distribution from our observations favors the first explanation.

In addition, a water maser (59.5 km s^{-1}) coincides with the ridge between S-B and the shocked gas of S-A. Since this maser is variable (Wang et al. 2006, 2012), it is not clear which source it relates to, but its presence marks the existence of a protostellar outflow.

4.4. A Global Picture of the 70 μm Dark G28.34 S

The high-mass cores S-A and S-B resolved from SMA observations are located at the southern edge of IRDC G28.34+0.06 (Feng et al. 2016). Aligned with the filament, they are consistent with the hierarchical fragmentation scheme found in the P1 clump (Wang et al. 2011, 2012; Zhang et al. 2015), which is 1′ to the NW and has several co-existing bipolar, jet-like, CO outflows. The W–E oriented outflow found in S-A also has other similarities to the outflows in P1. In particular, all outflows have orientations almost perpendicular to the major axis of the filament. However, the momentum, mechanical luminosity, and flow mass entrainment of the S-A outflow is at least one magnitude less intense than those found in P1, indicating the stellar object(s) in S-A is less evolved than the others in this IRDC. Despite the different outflow properties, S-A has a similar mass and IR properties to some other IR-dark cores embedded in P1. This indicates that the stellar object(s) in S-A is less evolved than the others in this IRDC. Similar outflows have also been reported in other IR-dark and IR-bright cores embedded in the IRDC "Snake" (Wang et al. 2014).

The total bolometric luminosity found in G28.34 S is low (10 $L_\odot$), which makes it intriguing to find an outflow in a 0.1 pc unresolved young high-mass star-forming core such as S-A. More importantly, the outflows detected in P1 and S-A indicate that a mechanical energy feeds back to the cores which are still dark at 70 μm. What is the mechanism that drives the outflows? What is the evolutionary status of these cores? How many protostellar objects have been formed but do not yet globally heat up the parental molecular clump (see more discussion on localized outflow heating in G28.34-P1 in Wang et al. 2012)?

We note that a recent large survey on scales of 0.5–1 pc presents detections of SiO $J = 2 \rightarrow 1$ and $J = 5 \rightarrow 4$ from many IR-quiet clumps (Csengeri et al. 2016). More specifically, 25% of those observed IR-quiet clumps present high-velocity $J = 2 \rightarrow 1$ line wings, indicating outflows. High-mass molecular gas cores may spend considerable life time in the stage which exhibits low luminosity, but already has active star-formation and outflow activities. The source S-A may represent the earliest part of this evolutionary stage.

5. CONCLUSION

We present NOEMA and IRAM 30 m observations that uncover the presence of at least one bipolar outflow in a 70 μm dark core G28.34 S-A. Revealed by shocked gas as high-velocity red/blueshifted lobes of SiO $J = 2 \rightarrow 1$, this W–E oriented outflow is also shown by the blueshifted gas lobe of SiO $J = 5 \rightarrow 4$ (from ALMA cycle 0 archival data). The PV diagram of this outflow indicates that the higher velocity components are closer to the continuum center. Moreover, the momentum, mechanism luminosity, and mass entrainment of this outflow in such a low-luminosity core indicate the center source(s) is in an early evolutionary stage of forming high-mass protostar(s). In addition, blue and redshifted gas reveal low-velocity elongation in the NW–SE orientation, which may be from a second outflow. Furthermore, we discuss the possible accretion scenarios of the outflow-powering young stellar object. We argue that the molecular line emission and the molecular outflows may provide a better indication of the accretion history of the forming young stellar object and thereby the evolutionary stage, than snapshot observations of the present bolometric luminosity.

We would like to thank the SMA staff and IRAM 30 m staff for their helpful support during the performance of telescopes in service mode. We thank Jan-Martin Winters for helping with the NOEMA data reduction. We thank Paola Caselli, Jaime Pineda, and Sarah Ragan for helpful discussion.

This research made use of NASA's Astrophysics Data System.

Z.Y.Z. acknowledges support from the European Research Council (ERC) in the form of Advanced Grant, COSMICISM. K.W. acknowledges support from grant WA3628-1/1 of the German Research Foundation (DFG) through the priority program 1573 ("Physics of the Interstellar Medium").

REFERENCES

Anderl, S., Guillet, V., Pineau des Forêts, G., & Flower, D. R. 2013, A&A, 556, A69
Arce, H. G., Shepherd, D., Gueth, F., et al. 2007, in Protostars and Planets V, ed. V. B. Reipurth, D. Jewitt, & K. Keil (Tucson, AZ: Univ. Arizona Press), 245
Beuther, H., Schilke, P., Sridharan, T. K., et al. 2002, A&A, 383, 892
Beuther, H., Zhang, Q., Greenhill, L. J., et al. 2004, ApJL, 616, L31
Bonnell, I. A., Bate, M. R., Clarke, C. J., & Pringle, J. E. 2001, MNRAS, 323, 785
Bonnell, I. A., Larson, R. B., & Zinnecker, H. 2007, in Protostars and Planets V, ed. V. B. Reipurth, D. Jewitt, & K. Keil (Tucson, AZ: Univ. Arizona Press), 149
Bonnell, I. A., Vine, S. G., & Bate, M. R. 2004, MNRAS, 349, 735
Butler, M. J., & Tan, J. C. 2009, ApJ, 696, 484
Carey, S. J., Clark, F. O., Egan, M. P., et al. 1998, ApJ, 508, 721
Carey, S. J., Feldman, P. A., Redman, R. O., et al. 2000, ApJL, 543, L157
Carey, S. J., Noriega-Crespo, A., Mizuno, D. R., et al. 2009, PASP, 121, 76
Caselli, P., Hartquist, T. W., & Havnes, O. 1997, A&A, 322, 296
Chen, H.-R., Liu, S.-Y., Su, Y.-N., & Zhang, Q. 2010, ApJL, 713, L50
Chira, R.-A., Beuther, H., Linz, H., et al. 2013, A&A, 552, A40
Csengeri, T., Leurini, S., Wyrowski, F., et al. 2016, A&A, 586, A149
Cyganowski, C. J., Whitney, B. A., Holden, E., et al. 2008, AJ, 136, 2391
Draine, B. T. 2011, Physics of the Interstellar and Intergalactic Medium (Princeton, NJ: Princeton Univ. Press)
Duarte-Cabral, A., Bontemps, S., Motte, F., et al. 2014, A&A, 570, A1
Dunham, M. M., & Vorobyov, E. I. 2012, ApJ, 747, 52
Egan, M. P., Shipman, R. F., Price, S. D., et al. 1998, ApJL, 494, L199
Feng, S., Beuther, H., Zhang, Q., et al. 2016, A&A, 592, A21
Fontani, F., Palau, A., Caselli, P., et al. 2011, A&A, 529, L7
Gong, H., & Ostriker, E. C. 2011, ApJ, 729, 120
Guillet, V., Jones, A. P., & Pineau des Forêts, G. 2009, A&A, 497, 145
Guillet, V., Pineau des Forêts, G., & Jones, A. P. 2011, A&A, 527, A123
Gusdorf, A., Cabrit, S., Flower, D. R., & Pineau des Forêts, G. 2008, A&A, 482, 809
Hirano, N., Liu, S.-Y., Shang, H., et al. 2006, ApJL, 636, L141

Hirano, N., Mikami, H., Umemoto, T., Yamamoto, S., & Taniguchi, Y. 2001, ApJ, 547, 899
Ho, P. T. P., Moran, J. M., & Lo, K. Y. 2004, ApJL, 616, L1
Hosokawa, T., Omukai, K., Yoshida, N., & Yorke, H. W. 2011, Sci, 334, 1250
Hosokawa, T., Yorke, H. W., & Omukai, K. 2010, ApJ, 721, 478
Jiménez-Serra, I., Caselli, P., Tan, J. C., et al. 2010, MNRAS, 406, 187
Jiménez-Serra, I., Martín-Pintado, J., Caselli, P., Viti, S., & Rodríguez-Franco, A. 2009, ApJ, 695, 149
Jiménez-Serra, I., Martín-Pintado, J., Rodríguez-Franco, A., & Marcelino, N. 2004, ApJL, 603, L49
Johnston, K. G., Robitaille, T. P., Beuther, H., et al. 2015, ApJL, 813, L19
Juvela, M., & Ysard, N. 2011, ApJ, 739, 63
Kong, S., Tan, J. C., Caselli, P., et al. 2016, ApJ, 821, 94
Krumholz, M. R., Bate, M. R., Arce, H. G., et al. 2014, in Protostars and Planets VI, ed. H. Beuther (Tucson, AZ: Univ. Arizona Press), 243
Krumholz, M. R., & Bonnell, I. A. 2007, arXiv:0712.0828
Krumholz, M. R., McKee, C. F., & Klein, R. I. 2005, ApJL, 618, L33
Kuiper, R., & Klessen, R. S. 2013, A&A, 555, A7
Lee, C.-F., Ho, P. T. P., Palau, A., et al. 2007, ApJ, 670, 1188
Leurini, S., Codella, C., López-Sepulcre, A., et al. 2014, A&A, 570, A49
Liu, H. B., Jiménez-Serra, I., Ho, P. T. P., et al. 2012, ApJ, 756, 10
Liu, H. B., Takami, M., Kudo, T., et al. 2016, SciA, 2, e1500875
López-Sepulcre, A., Watanabe, Y., Sakai, N., et al. 2016, ApJ, 822, 85
McKee, C. F., & Tan, J. C. 2003, ApJ, 585, 850
McMullin, J. P., Waters, B., Schiebel, D., Young, W., & Golap, K. 2007, in ASP Conf. Ser. 376, Astronomical Data Analysis Software and Systems XVI, ed. R. A. Shaw, F. Hill, & D. J. Bell (San Francisco, CA: ASP), 127
Mikami, H., Umemoto, T., Yamamoto, S., & Saito, S. 1992, ApJL, 392, L87
Nguyen-Lu'o'ng, Q., Motte, F., Carlhoff, P., et al. 2013, ApJ, 775, 88
Ossenkopf, V., & Henning, T. 1994, A&A, 291, 943
Palau, A., Ho, P. T. P., Zhang, Q., et al. 2006, ApJL, 636, L137
Pillai, T., Wyrowski, F., Carey, S. J., & Menten, K. M. 2006, A&A, 450, 569
Qiu, K., Zhang, Q., Beuther, H., & Yang, J. 2007, ApJ, 654, 361
Ragan, S., Henning, T., Krause, O., et al. 2012, A&A, 547, A49
Ragan, S. E., Bergin, E. A., & Gutermuth, R. A. 2009, ApJ, 698, 324
Ragan, S. E., Henning, T., & Beuther, H. 2013, A&A, 559, A79
Rathborne, J. M., Jackson, J. M., & Simon, R. 2006, ApJ, 641, 389
Robitaille, T. P., Meade, M. R., Babler, B. L., et al. 2008, AJ, 136, 2413
Russeil, D., Zavagno, A., Motte, F., et al. 2010, A&A, 515, A55
Schilke, P., Walmsley, C. M., Pineau des Forets, G., & Flower, D. R. 1997, A&A, 321, 293
Schuller, F., Menten, K. M., Contreras, Y., et al. 2009, A&A, 504, 415
Simon, R., Jackson, J. M., Rathborne, J. M., & Chambers, E. T. 2006, ApJ, 639, 227
Sridharan, T. K., Beuther, H., Saito, M., Wyrowski, F., & Schilke, P. 2005, ApJL, 634, L57
Stahler, S. W., Shu, F. H., & Taam, R. E. 1980, ApJ, 241, 637
Tackenberg, J., Beuther, H., Henning, T., et al. 2012, A&A, 540, A113
Tan, J. C., Beltrán, M. T., Caselli, P., et al. 2014, in Protostars and Planets VI, ed. H. Beuther et al. (Tucson, AZ: Univ. Arizona Press), 149
Tan, J. C., Kong, S., Butler, M. J., Caselli, P., & Fontani, F. 2013, ApJ, 779, 96
Tan, J. C., & McKee, C. F. 2002, in ASP Conf. Ser. 267, Hot Star Workshop III: The Earliest Phases of Massive Star Birth, ed. P. Crowther (San Francisco, CA: ASP), 267
Teyssier, D., Hennebelle, P., & Pérault, M. 2002, A&A, 382, 624
Toomre, A. 1964, ApJ, 139, 1217
Vasyunina, T., Linz, H., Henning, T., et al. 2009, A&A, 499, 149
Vorobyov, E. I., Baraffe, I., Harries, T., & Chabrier, G. 2013, A&A, 557, A35
Vorobyov, E. I., & Basu, S. 2015, ApJ, 805, 115
Wang, K., Zhang, Q., Testi, L., et al. 2014, MNRAS, 439, 3275
Wang, K., Zhang, Q., Wu, Y., Li, H.-b., & Zhang, H. 2012, ApJL, 745, L30
Wang, K., Zhang, Q., Wu, Y., & Zhang, H. 2011, ApJ, 735, 64
Wang, Y., Zhang, Q., Pillai, T., Wyrowski, F., & Wu, Y. 2008, ApJL, 672, L33
Wang, Y., Zhang, Q., Rathborne, J. M., Jackson, J., & Wu, Y. 2006, ApJL, 651, L125
Wienen, M., Wyrowski, F., Schuller, F., et al. 2012, A&A, 544, A146
Zhang, Q., Ho, P. T. P., Wright, M. C. H., & Wilner, D. J. 1995, ApJL, 451, L71
Zhang, Q., Wang, K., Lu, X., & Jiménez-Serra, I. 2015, ApJ, 804, 141
Zhang, Q., Wang, Y., Pillai, T., & Rathborne, J. 2009, ApJ, 696, 268